Event-Triggered Distributed MPC for CPSs With Coupled Dynamics: A Coupling Separation and Compensation Technique

Tao Wang, Yu Kang, *Senior Member, IEEE*, Pengfei Li, and Yun-Bo Zhao

***Abstract*—A novel event-triggered distributed model predictive control strategy incorporating a coupling separation and compensation technique is developed for cyber-physical systems (CPSs) with coupled dynamics. This strategy separates mutual disturbances caused by dynamic coupling into matched and unmatched components. The matched coupling is compensated using a pre-designed control input, whereas unmatched coupling is alleviated by optimizing the selection of a separation matrix. In this way, the impact of mutual disturbances is reduced, thereby enhancing prediction precision, which in turn leads to a notable reduction in triggering frequency. Moreover, a newly developed tightened state constraint, which incorporates the triggering threshold, is designed to ensure the satisfaction of the actual state constraint. The recursive feasibility and stability analysis is conducted, supported by numerical simulations of a nonlinear CPS that demonstrate the effectiveness of the proposed strategy.**

***Index Terms*—Cyber-physical systems (CPSs), distributed model predictive control, event-triggered control, separation and compensation technique.**

Nomenclature

δ_i	Control parameter related to trigger threshold.
$\hat{u}_i, \hat{x}_i$	Predicted control input and state trajectory.
$\hat{v}_i^*, \hat{x}_i^*$	Optimal predicted control input and state trajectory.
$\mathcal{N}_i$	Neighbor set of subsystem i.
$\mathcal{U}_i, \mathcal{X}_i$	Control constraint and state constraint of subsystem i.
$\phi_i(\alpha_i\varepsilon_i)$	Terminal state constraint.
$\psi(\cdot), \varphi(\cdot)$	Stage cost function and terminal cost function.
ρ_i	Control parameter of the consistency constraint.
$\sum_{j\in\mathcal{N}_i} g_{ij}^M(x_j)$	Matched coupling.
$\sum_{j\in\mathcal{N}_i} g_{ij}^U(x_j)$	Unmatched coupling.
Ξ_i	Tightened constraint set.
$L_{f_i}, L_{g_{ij}}$	Lipschitz constant.
N_a	Number of subsystems.
N_i	Number of neighbors of subsystem i.
Q_i, R_i, P_i	Cost function weighting matrices.
T_p	Prediction horizon.
u_i^M	Control input for compensating matched coupling.

Received 12 November 2024; revised 28 May 2025; accepted 23 September 2025. Date of publication 26 September 2025; date of current version 28 October 2025. This work was supported in part by the National Natural Science Foundation of China under Grant 62033012, Grant 62473352, Grant 62173317, and Grant 62103394, in part by Academic Newcomer Promotion Program under Grant JZ2024HGTA0183, in part by University Synergy Innovation Program of Anhui Province, China, under Grant GXXT-2023-068. *(Corresponding author: Yu Kang.)*

Tao Wang is with the Department of Automation, Hefei University of Technology, Hefei 230009, China (e-mail: wanghtao@mail.ustc.edu.cn).

Yu Kang is with the Department of Automation, University of Science and Technology of China, Hefei 230027, China, also with Hefei University of Technology, Hefei 230009, China, and also with the Institute of Artificial Intelligence, Hefei Comprehensive National Science Center, Hefei 230088, China (e-mail: kangduyu@ustc.edu.cn).

Pengfei Li and Yun-Bo Zhao are with the Department of Automation, University of Science and Technology of China, Hefei 230027, China (e-mail: uffylee@ustc.edu.cn; ybzhao@ustc.edu.cn).

Digital Object Identifier 10.1109/TICPS.2025.3614594

I. Introduction

CYBER-PHYSICAL systems (CPSs), which achieve a high degree of integration of physical resources and cyber information resources, have received increasing attention [1]. CPSs have found many applications in the era of Industry 4.0, such as industry control, energy, intelligent transportation, and smart grid [2]. In practical applications, CPSs such as power grids, and intelligent transportation systems, are characterized by being distributed and spatially interconnected [3]. These type of CPSs cover vast areas and consist of numerous interacting components, creating extensive communication needs and computational demands that challenge centralized control. Physical constraints further complicate matters. In this context, distributed approaches, such as distributed model predictive control (MPC), have thus become prominent. In distributed MPC, local optimization problems subject to system constraints are solved, with decision information exchanged among neighboring nodes at each time step. This enables local controllers to operate subsystems autonomously while coordinating with adjacent nodes, thereby alleviating overall computational and communication loads [4]. In recent years, distributed MPC has been widely used in CPSs [5], [6].

Designing distributed MPC for such type of CPSs with physically coupled dynamics is complex because the dynamic coupling between subsystems impacts optimization feasibility and system stability. In this context, dealing with dynamic coupling can be divided into two main routes. One route employs

the nominal system model, which ignores coupling terms, to predict the future trajectory of the system, as seen in tube-based MPC [7], MPC with robustness constraints [4], and cooperative optimization-based distributed MPC scheme [8]. While using a nominal model simplifies design, it ignores information exchange that could enhance performance.

The second route enhances performance through information exchange. Typically, this involves incorporating the assumed state of neighboring subsystems into the predicted model to improve prediction precision [9], [10], [11]. However, ensuring recursive feasibility and stability is challenging due to mutual disturbances from coupling. Solutions include consistency constraints [9], robustness constraints [10], and Lyapunov-based schemes [11], along with iterative learning [12] and data-driven methods [13]. The works mentioned above employ time-triggered schemes, which solve local optimization problems and exchange information periodically, leading to unnecessary utilization of communication resources. However, communication resources are limited in CPSs in some situation, particularly when the communication network is shared among multiple devices [14]. Therefore, the time-triggered MPC scheme is no longer suitable, and a resource-aware strategy is needed to schedule data transmission only when necessary.

Event-triggered distributed MPC (ET-DMPC) is a promising approach to address this challenge, as it operates data transmission only when the pre-designed triggering conditions are satisfied. In ET-DMPC literature, designing triggering conditions is crucial as it affects the recursive feasibility of the optimization problem and system stability [15]. For CPSs with coupled dynamics, creating an effective ET-DMPC strategy is challenging because dynamic coupling can cause mutual disturbances, threatening feasibility and stability. As a result, literature is scarce on the topic. For linear interconnected systems, see [16], [17]; for nonlinear interconnected systems, see [18], [19]. In these works, the triggering condition typically involves comparing the error between the actual state and the predicted one with a triggering threshold. Therefore, in order to reduce the triggering frequency and thus alleviate communication load, two alternative methods can be employed: 1) enhancing the prediction precision, thereby reducing the error between the actual state and the predicted one, and 2) increasing the triggering threshold. Although incorporating the assumed state information of neighbors into the predicted model can enhance performance to some extent, the inaccuracies in this assumed state information still lead to prediction errors. Additionally, for nonlinear coupled systems, the state constraints are not considered.

Motivated by the above discussion, this paper investigates ET-DMPC for nonlinear CPSs with coupled dynamics, and a novel ET-DMPC strategy that incorporates a coupling separation and compensation technique (CSCT) is proposed. The main contributions of this paper are summarized as follows:

- A novel distributed MPC scheme is proposed, where the CSCT enhances prediction precision and allows a stronger degree of coupling, and a newly developed tightened state constraint ensures the satisfaction of the actual state constraint.
- A new triggering condition is designed, featuring a variable and less conservative threshold, which effectively reduces the frequency of triggering events.
- The recursive feasibility and the stability under the proposed CSCT-based ET-DMPC strategy are rigorously analyzed and established.

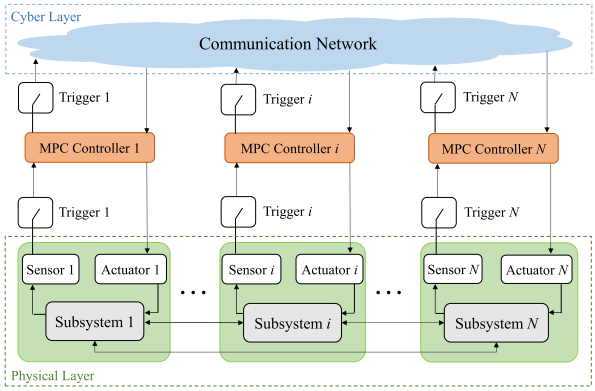

Fig. 1. The framework of CPSs equipped with ET-DMPC.

Notations: Let $\mathbb{R}$ represent the set of real numbers and $\mathbb{N}$ the set of nonnegative integers, with $\mathbb{R}^n$ denoting the n-dimensional Euclidean space. For a given matrix P, $P \succ 0$ indicates that P is positive definite. For a vector x, its Euclidean norm is denoted by $\|x\| = \sqrt{x^T x}$, and the P-weighted norm is represented by $\|x\|_P = \sqrt{x^T P x}$. For two sets $A, B \subseteq \mathbb{R}^n$, the Pontryagin difference set is defined as $A \ominus B = \{a : a + b \in A, \forall b \in B\}$, and the Minkowski addition set is $A \oplus B := \{a + b : a \in A, b \in B\}$.

II. Problem Formulation

The framework of the ET-DMPC for CPSs is depicted in Fig. 1. The local plants are located at the physical layer, and the information exchange occurs at the cyber layer.

The CPS under consideration is an input-affine nonlinear system, composed of N subsystems, each governed by its own dynamics but interacting with neighboring subsystems. The dynamics of subsystem i is formulated as

$$x_i(k+1) = f_i(x_i(k)) + B_i(x_i(k))u_i(k) + \sum_{j \in \mathcal{N}_i} g_{ij}(x_j(k)) + \omega_i(k) \tag{1}$$

where $i \in \mathcal{N} = \{1, \ldots, N_a\}$, the state $x_i(k) \in \mathbb{R}^{n_i}$ and control input $u_i(k) \in \subset \mathbb{R}^{m_i}$ are subjected to the following constraint

$$x_i(k) \in \mathcal{X}_i, \quad u_i(k) \in \mathcal{U}_i \tag{2}$$

where the sets $\mathcal{X}_i$ and $\mathcal{U}_i$ are compact, and $\{0\} \subseteq \mathcal{X}_i$ and $\{0\} \subseteq \mathcal{U}_i$. The matrix $B \in \mathbb{R}^{n_i \times m_i}$ and $\text{rank}(B_i(x_i)) = m_i$. The set $\mathcal{N}_i$ represents the neighbor set of subsystem i, defined as $\mathcal{N}_i =$

$\{j \in \mathcal{N} \setminus \{i\} \mid g_{ij} \neq 0\}$. The disturbance $\omega_i(k)$ belongs to the set $\mathcal{W}_i = \{\omega_i \in \mathbb{R}^{n_i} \mid \|\omega_i\|_{P_i} \leq \xi_i, \xi_i > 0\}$.

The nominal dynamics of system (1) is defined by ignoring the disturbance:

$$\hat{x}_i(k+1) = f_i(\hat{x}_i(k)) + B_i(\hat{x}_i(k))u_i(k) + \sum_{j\in\mathcal{N}_i} g_{ij}(\hat{x}_j(k)) \quad (3)$$

where $\hat{x}_i(k)$ is the nominal state. The nominal system satisfies the following assumption.

Assumption 1: There exists a constant $L_{f_i} > 0$ such that $\|f_i(x) + B_i(x)u - f_i(z) - B_i(z)u\|_{P_i} \leq L_{f_i}\|x - z\|_{P_i}$, $\forall x, z \in \mathcal{X}_i$ and $u \in \mathcal{U}_i$.

Let k_i^m ($m \in \mathbb{N}$) denote the m-th triggering instant for subsystem i, a primal local optimization problem for the subsystem i at k_i^m can be formulated as

$$\min_{\hat{\mathbf{u}}_i(k_i^m)} J_i(\hat{x}_i(k_i^m + l|k_i), \hat{u}_i(k_i^m + l|k_i))$$

$$\text{s.t. } \hat{x}_i(k_i^m + l + 1|k_i^m) = f_i(\hat{x}_i(k_i^m + l|k_i^m)) + \sum_{j\in\mathcal{N}_i} g_{ij}(\hat{x}_j(k_i^m + l|k_i^m)) + B_i(\hat{x}_i(k_i^m + l|k_i^m))\hat{u}(k_i^m + l|k_i^m), \quad (4a)$$

$$\hat{x}(k_i^m + l|k_i^m) \in \mathcal{X}_i \quad (4b)$$

$$\hat{u}(k_i^m + l|k_i^m) \in \mathcal{U}_i \quad (4c)$$

$$\hat{x}_i(k_i^m + T_p|k_i) \in \phi_i(\alpha_i\varepsilon_i), \quad (4d)$$

where $l = 0, \ldots, T_p - 1$, T_p is the prediction horizon, $J_i(\hat{x}_i(k_i^m + l|k_i^m), \hat{u}_i(k_i^m + l|k_i^m))$ is the cost function, $\hat{\mathbf{u}}_i(k_i^m) = \{\hat{u}_i(k_i^m|k_i^m), \ldots, \hat{u}_i(k_i^m + T_p|k_i^m)\}$ is the predicted control input sequence, $\hat{\mathbf{x}}_i(k_i^m) = \{\hat{x}_i(k_i^m|k_i^m), \ldots, \hat{x}_i(k_i^m + T_p|k_i^m)\}$ is the corresponding predicted state sequence, and $\phi_i(\alpha_i\varepsilon_i) = \{x_i : \|x_i\|_{P_i} \leq \alpha_i\varepsilon_i\}$ is the terminal state constraint with two constants $0 < \alpha_i < 1$ and $\varepsilon_i > 0$.

The primal triggering condition is given similarly to many event-triggered MPC works, that is, by comparing the error between the actual state and the predicted state [15], [18].

$$\|x_i(k) - \hat{x}_i(k|k_i^m)\| > \sigma_i \quad (5)$$

where σ_i is a constant triggering threshold.

Based on the above preliminaries, the entire execution process of Fig. 1 can be described as follows. At each triggering time k_i^m, sensor i samples the current state of subsystem i, i.e., $\hat{x}(k_i^m)$. Subsequently, trigger i evaluates if an event has been triggered according to the triggering condition (5). If the condition (5) is satisfied, MPC controller i solves the corresponding optimization problem (4), yielding the predicted control input sequence $\hat{\mathbf{u}}_i(k_i)$ and the predicted state sequence $\hat{\mathbf{x}}_i(k_i)$. Simultaneously, the state information $\hat{\mathbf{x}}_i(k_i)$ is transmitted to neighboring subsystems $j \in \mathcal{N}_i$ through the communication network. Otherwise, no information is transmitted.

It is worth noting that the primary event-triggered strategy faces three main issues:

i) The neighbor's predicted state $\hat{x}_j(k_i^m + l|k_i^m)$ in (4a) cannot be obtained due to the asynchronous communication between subsystems;

ii) The actual state constraint $x_i(k) \in \mathcal{X}_i$ cannot be guaranteed through the constraint (4b) due to the potential predicted errors between $x_i(k)$ and $\hat{x}_i(k|k_i^m)$ caused by the disturbance;

iii) The triggering condition defined by (5) may be triggered too frequently if the prediction is not sufficiently accurate.

Our objective is to design an ET-DMPC strategy for system (1) that ensures the stability of system (1) while alleviating the communication burden. Specifically, the following issues will be addressed:

i) Design a distributed scheme to enable the use of information from neighboring subsystems in implementing the distributed MPC algorithm.

ii) Reconstruct the state constraint (4b) to ensure that the actual state constraint (2) is satisfied while guaranteeing that the redesigned optimization problem is recursively feasible.

iii) Enhance the prediction precision to reduce the triggering frequency.

III. CSCT-Based Event-Triggered Distributed MPC

In this section, we first propose the CSCT to implement the distributed MPC algorithm and enhance the prediction precision. Then, a novel ET-DMPC strategy based on the proposed CSCT is designed.

A. Coupling Separation and Compensation Technique

Since the triggering instants are distinct for different subsystems, i.e., an asynchronous triggering mechanism, each subsystem i, $i \in \mathcal{N}$ cannot obtain its neighbor's predicted state $\hat{x}_j(k_i^m + l|k_i^m)$ at triggering instant k_i^m. Consequently, to implement the distributed MPC algorithm, some studies have employed a constructed assumed state trajectory of neighboring subsystem $j \in \mathcal{N}_i$, denoted by $\tilde{\mathbf{x}}_j(k_i^m)$, prior to each triggering instant, see, e.g., [9], [20]. And the assumed state trajectory $\tilde{\mathbf{x}}_j(k_i^m)$ at k_i^m is typically constructed using the solution from the previous triggering instant before k_i^m, such as $\tilde{x}_j(k_i^m + l|k_i^m) = \hat{x}_i(k_i^m + l|k_i^{m-1})$.

However, there still exists a discrepancy between the predicted state $\hat{x}_j(k_i^m + l|k_i^m)$ and the assumed state $\tilde{x}_j(k_i^m + l|k_i^m)$ due to the disturbance ω_i, leading to a deviation between the actual state $x_i(k)$ and the predicted state $\hat{x}_i(k|k_i^m)$. According to the triggering condition (5), a larger deviation results in more frequent triggering events. To address this issue, a promising approach is to mitigate the impact of mutual disturbances caused by dynamic coupling $\sum_{j\in\mathcal{N}_i} g_{ij}(x_j(k))$. To this end, the CSCT is proposed.

First, by separating the unmatched coupling $\sum_{j\in\mathcal{N}_i} g_{ij}^U(x_j(k))$ $\left(\sum_{j\in\mathcal{N}_i} g_{ij}^U(x_j(k)) \notin \text{Range}(B_i(x_i(k))), \exists x_i \in \mathcal{X}_i\right)$ from the matched coupling $\sum_{j\in\mathcal{N}_i} g_{ij}^M(x_j(k))$ $\left(\sum_{j\in\mathcal{N}_i} g_{ij}^M(x_j(k)) \in \text{Range}(B_i(x_i(k))), \forall x_i \in \mathcal{X}_i\right)$, the dynamical coupling $\sum_{j\in\mathcal{N}_i} g_{ij}(x_j(k))$ can be expressed as:

$$\sum_{j\in\mathcal{N}_i} g_{ij}(x_j(k)) = \sum_{j\in\mathcal{N}_i} g_{ij}^M(x_j(k)) + \sum_{j\in\mathcal{N}_i} g_{ij}^U(x_j(k)) \quad (6a)$$

$$\sum_{j\in\mathcal{N}_i} g_{ij}^M(x_j(k)) = B_i(x_i(k))H_i(x_i(k)) \sum_{j\in\mathcal{N}_i} g_{ij}(x_j(k)) \quad (6b)$$

$$\sum_{j\in\mathcal{N}_i} g_{ij}^U(x_j(k)) = (I - B_i(x_i(k))H_i(x_i(k))) \sum_{j\in\mathcal{N}_i} g_{ij}(x_j(k)) \quad (6c)$$

where $H_i(x_i(k))$ is a sate-dependent matrix. The unmatched coupling g_{ij}^U satisfies the following assumption.

Assumption 2: The functions g_{ij}^U is Lipschitz continuous with a constant $L_{g_{ij}} > 0$, i.e., $\|g_{ij}^U(x) - g_{ij}^U(z)\|_{P_i} \le L_{g_{ij}} \|x - z\|_{P_i}$, $\forall x, z \in \mathcal{X}_j$ and $u \in \mathcal{U}_i$

Remark 1: Assumptions 2 is mild, as shown in [18], [21]. Unlike the aforementioned works, which assume that $\|g_{ij}(x) - g_{ij}(z)\|_{P_i} \le \bar{L}_{g_{ij}} \|x - z\|_{P_i}$, this paper adopts a less conservative approach so that $L_{g_{ij}} \le \bar{L}_{g_{ij}}$. Particularly, if $\sum_{j\in\mathcal{N}_i} g_{ij}(x_j(k))$ is matched coupling, then $L_{g_{ij}} \equiv 0$. Consequently, to ensure recursive feasibility, a larger triggering threshold can be achieved, see Section IV for details.

Remark 2: In practical CPSs, dynamic coupling phenomena are common but can often be separated and compensated through CSCT. A representative example is thermal power grid systems [11], [22], where inter-area frequency deviations exhibit dynamic interdependencies due to power exchange mechanisms between adjacent subsystems. Another characteristic case emerges in cascaded continuous stirred tank reactors (CSTRs) [23], where the ith reactor's concentration and thermal states demonstrate direct propagation effects from the preceding $(i-1)$th unit through material flow and heat transfer processes. Notably, certain CPSs exhibit fully matched coupling, such as multi-area nonlinear power systems [22], chemical processes [23], and building temperature control scenarios [24].

Second, to mitigate the impact of mutual disturbances, we compensate for matched coupling and minimize unmatched coupling. The matched coupling can be offset by feedforward compensation, whereas the unmatched coupling cannot be directly compensated. To address the matched coupling, the control input is divided into two components of the following form:

$$u_i(k) = \upsilon(k) + u_i^M(k) \quad (7)$$

where $\upsilon(k)$ is obtained by solving the following redesigned optimization problem, and $u_i^M(k)$, is utilized to compensate for matched coupling, takes the following form:

$$u_i^M(k) = -H_i(x_i(k)) \sum_{j\in\mathcal{N}_i} g_{ij}(x_j(k)) \quad (8)$$

Additionally, the above two control inputs are subject to the following constraints to ensure that $u_i(k) \in \mathcal{U}_i$ is satisfied.

$$\upsilon(k) \in \mathcal{U}_i - \mathcal{V}_i,\ u_i^M(k) \in \mathcal{V}_i \quad (9)$$

Substituting (7) and (8) into (3), the nominal model becomes

$$x_i(k+1) = f_i(x_i(k)) + B_i(x_i(k))\upsilon(k) + \sum_{j\in\mathcal{N}_i} g_{ij}^U(x_j(k)) \quad (10)$$

From the coupling separation (6), it can be seen that the state-dependent matrix $H_i(x_i(k))$ plays an important role in mitigating the impact of mutual disturbances. To reject the unmatched coupling, we can choose a suitable $H_i(x_i)$, which is shown in the following Lemma 1.

Lemma 1: The unmatched coupling $g_{ij}^U(x_j)$ can be minimized by selecting $H_i(x_i) = (B_i(x_i)^T P_i B_i(x_i))^{-1} B_i(x_i)^T P_i$, i.e.,

$$(B_i(x_i)^T P_i B_i(x_i))^{-1} B_i(x_i)^T P_i = \arg\min_{H_i(x_i)} \|(I - B_i(x_i)H_i(x_i)) \sum_{j\in\mathcal{N}_i} g_{ij}(x_j)\|_{P_i} \quad (11)$$

Proof: The proof follows a similar line as the proof of the Proposition 2 in [25], thus we give a brief outline here.

Let M_i is a matrix such that $M_i^T M_i = P_i$, it follows that

$$\|(I - B_i(x_i)H_i(x_i)) \sum_{j\in\mathcal{N}_i} g_{ij}(x_j(k))\|_{P_i} = \|M_i(I - B_i(x_i)H_i(x_i)) \sum_{j\in\mathcal{N}_i} g_{ij}(x_j(k))\|_2$$

Let $\chi_i = M_i \sum_{j\in\mathcal{N}_i} g_{ij}(x_j)$ and $\Omega_i = H_i(x_i) \sum_{j\in\mathcal{N}_i} g_{ij}(x_j)$, problem (11) is rewritten as

$$\min_{\Omega_i\in\mathbb{R}^{m_i}} \|(\chi_i - M_i B_i(x_i)\Omega_i\|_2$$

which, according to [25] has the optimal solution $\Omega_i^* = (B_i(x_i)^T M_i^T M_i B_i(x_i))^{-1} B_i(x_i)^T M_i^T \chi_i$. Selecting $H_i(x_i) = (B_i(x_i)^T P_i B_i(x_i))^{-1} B_i(x_i)^T P_i$, we have

$$\Omega_i = (B_i(x_i)^T P_i B_i(x_i))^{-1} B_i(x_i)^T P_i \sum_{j\in\mathcal{N}_i} g_{ij}(x_j) = \Omega_i^*$$

which implies (11) is true. ■

B. Event-Triggered Distributed MPC Algorithm

Optimization problem: With the above preliminaries, the optimization problem based on CSCT is finally designed as

$$\min_{\hat{\mathbf{v}}_i(k_i^m)} J_i(\hat{x}_i(k_i^m + l|k_i^m), \hat{v}_i(k_i^m + l|k_i^m))$$

subject to:

$$\hat{x}_i(k_i^m + l + 1|k_i^m) = f_i(\hat{x}_i(k_i^m + l|k_i^m)) + \sum_{j\in\mathcal{N}_i} g_{ij}^U(\tilde{x}_j(k_i^m + l|k_i^m)) + B_i(\hat{x}_i(k_i^m + l|k_i^m))\hat{v}(k_i^m + l|k_i^m), \quad (12a)$$

$$\hat{x}(k_i^m + l|k_i^m) \in \Xi_i(l), l = 1, \ldots, T_p - 1 \quad (12b)$$

$$\hat{v}(k_i^m + l|k_i^m) \in \mathcal{U}_i - \mathcal{V}_i, l = 0, \ldots, T_p - 1 \quad (12c)$$

$$\|\hat{x}_i(k_i^m + l|k_i^m) - \hat{x}_i^*(k_i^m + l|k_i^m)\|_{P_i} \le \rho_i, l = 1, \ldots, T_p \quad (12d)$$

$$\hat{x}_i(k_i^m + T_p|k_i^m) \in \phi_i(\alpha_i\varepsilon_i), \quad (12e)$$

where $\hat{x}_i(k_i^m|k_i^m) = x(k_i^m)$.

The cost function is defined as

$$J_i(\hat{x}_i(k_i^m + l|k_i^m), \hat{v}_i(k_i^m + l|k_i^m))$$

$$= \sum_{l=0}^{T_p-1} \psi(\hat{x}_i(k_i^m+l|k_i^m), \hat{v}_i(k_i^m+l|k_i^m)) + \varphi(\hat{x}_i(k_i^m+T_p|k_i^m)), \tag{13}$$

where $\psi(x_i, v_i) = \|x_i\|^2_{Q_i} + \|v_i\|^2_{R_i}$ is the stage cost, $\varphi(x_i) = \|x_i\|^2_{P_i}$ is the terminal cost. $\hat{\mathbf{v}}_i^*(k_i{}^m) = \{\hat{v}_i^*(k_i{}^m|k_i^m), \ldots, \hat{v}_i{}^*(k_i{}^m + T_p - 1|k_i^m)\}$ is the optimal control input sequence at triggering instant $k_i{}^m$, and $\hat{\mathbf{x}}_i^*(k_i^m) = \{\hat{x}_i^*(k_i^m|k_i^m), \ldots, \hat{x}_i^*(k_i^m + T_p|k_i^m)\}$ is the corresponding predicted state. The superscript "*" denotes the optimal control input or state trajectory obtained by solving optimization problem (12).

The assumed state $\tilde{x}_j(k_i^m + l|k_i^m)$ is constructed by

$$\tilde{x}_j(k_i^m+l|k_i^m) = \begin{cases} \tilde{x}_j^*(k_i^m+l|\pi(k_i^m)), l=0,\ldots,T_p+\pi(k_i^m)-k_i^m \\ f_j(\tilde{x}_j(k_i^m+l-1|k_i^m))+B_jK_j\tilde{x}_j(k_i^m+l-1|k_i^m), \\ \quad l=T_p+\pi(k_i^m)-k_i^m+1,\ldots,T_p \end{cases} \tag{14}$$

where $\pi_j(k_i^m)$ denotes the triggering instant of subsystem j that is closest to k_i^m, i.e., $\pi_j(k_i^m) = \max\{k_j^m : k_j^m \le k_i^m\}$.

The tightened constraint set $\Xi_i(l)$ is designed as

$$\Xi_i(l) := \mathcal{X}_i \ominus \left\{x \in \mathbb{R}^{n_i} : \|x\|_{P_i} \le \frac{L_{f_i}^l - 1}{L_{f_i}-1}\eta_i + \frac{L_{f_i}^l - L_{f_i}}{(L_{f_i}-1)^2}T_pNL_{g_{ij}}\rho_j\right\}, \tag{15}$$

where the control parameters η_i and ρ_j are two constants and will be chosen in Section IV.

Equation (12a) represents the prediction model, which differs from the primal prediction model (4a). The time-varying tightened constraint (12b) is designed to ensure that the actual state constraint $x_i(k) \in \mathcal{X}_i$ is satisfied, as will be verified in Section IV. Additionally, consistency constraint (12d), which limits the deviation of the predicted state for two successive trigger instants, is introduced to guarantee the recursive feasibility of the optimization problem.

Assumption 3: There exists a set $\phi_i(\varepsilon_i)$, an auxiliary control law $K_i(x_i) : \phi_i(\varepsilon_i) \to \mathcal{U}_i - \mathcal{V}_i$, and a matrix $P_i \succ 0$ such that: (i) $\phi_i(\varepsilon_i) \subseteq \{x_i \in \Xi(T_p-1) : K_ix_i \in \mathcal{U}_i - \mathcal{V}_i\}$; (ii) $f_i(x_i) + B_i(x_i)K_i(x_i) + \sum_{j\in\mathcal{N}_i} g_{ij}^U(x_j) \in \phi_i(\alpha_i\varepsilon_i), \forall x_i \in \phi_i(\varepsilon_i), x_j \in \phi_j(\varepsilon_j)$; (iii) $\varphi(f_i(x_i) + B_i(x_i)K_i(x_i)) - \varphi(x_i) \le -\psi(x_i, K_i(x_i)), \forall x_i \in \phi_i(\varepsilon_i)$.

Remark 3: The assumed state trajectory $\tilde{x}_j$ is constructed based on the previously optimal state trajectory as in [9], [18]. Due to external perturbations and asynchronous communication, the assumed state deviates from the actual one. Unlike traditional methods that incorporate the entire uncertain coupling term, $\sum_{j\in\mathcal{N}_i} g_{ij}(\tilde{x}_j)$, in the predicted model, the proposed approach includes only the unmatched part, $\sum_{j\in\mathcal{N}_i} g_{ij}^U(\tilde{x}_j)$. Particularly, if $\sum_{j\in\mathcal{N}_i} g_{ij}(x_j(k))$ is matched coupling, then $\sum_{j\in\mathcal{N}_i} g_{ij}^U(\tilde{x}_j) \equiv 0$. Therefore, the impact of mutual interference is significantly reduced.

Remark 4: Assumption 3 is a standard assumption adopted in much DMPC literature to facilitate the feasibility and stability analysis, see, e.g., [17], [18], [21]. The parameters ε_i can be chosen following the similar line of the lemma 3.4 in [18]. Determining α_i analytically for a coupled nonlinear system is a difficult task. Instead, we can find α_i via numerical simulations. Specifically, after the parameter ε_i is determined, $0 < \alpha_i < 1$ is selected by numerical methods so that property (ii) in Assumption 3 can be satisfied.

Event-triggering strategy: The triggering condition, which determines the next triggering instant k_i^{m+1}, is designed in this part. First, we derive the state error between a candidate state $\bar{x}_i(k_i^{m+1}+l|k_i^{m+1})$ and the optimal state $\hat{x}_i{}^*(k_i{}^m + l|k_i{}^m)$ to facilitate the design of the triggering condition. Define $\bar{x}_i(k_i^{m+1}+l+1|k_i{}^{m+1}) = f_i(\bar{x}_i(k_i{}^{m+1}+l|k_i^{m+1})) + B_i(\bar{x}_i(k_i{}^{m+1}+l|k_i{}^{m+1}))\bar{v}_i(k_i{}^{m+1}+l|k_i^{m+1}) + \sum_{j\in\mathcal{N}_i} g_{ij}^U(\tilde{x}_j(k_i^{m+1}+l|k_i{}^{m+1}))$ and $\Delta(k_i^m) = k_i^{m+1} - k_i{}^m$, where the control input sequence $\bar{\boldsymbol{v}}_i(k_i{}^{m+1}+l|k_i^{m+1})$ is constructed as

$$\bar{v}_i(k_i^{m+1}+l|k_i^{m+1}) = \begin{cases} \hat{v}_i^*(k_i^m+l+\Delta(k_i^m)|k_i^m), l=0,\ldots,T_p-\Delta(k_i^m)-1 \\ K_ix_i^*(k_i^m+N|k_i^m), l=T_p-\Delta(k_i^m) \\ K_i\bar{x}_i(k_i^{m+1}+l|k_i^{m+1}), l=T_p-\Delta(k_i^m)+1,\ldots,T_p-1. \end{cases} \tag{16}$$

Define $N = \max_{i\in\mathcal{N}} \text{Card}\{\mathcal{N}_i\}$. We can obtain

$$\begin{aligned} &\|\bar{x}_i(k_i^{m+1}+l|k_i^{m+1}) - \hat{x}_i^*(k_i^{m+1}+l|k_i^m)\|_{P_i} \\ &\le L_{f_i}\|\bar{x}_i(k_i^{m+1}+l-1|k_i^{m+1}) - \hat{x}_i^*(k_i^{m+1}+l-1|k_i^m)\|_{P_i} \\ &\quad + NL_{g_{ij}}(\tilde{x}_j(k_i^{m+1}+l-1|k_i^{m+1}) - \tilde{x}_j(k_i^{m+1}+l-1|k_i^m)) \\ &\le L_{f_i}^l\|x_i(k_i^{m+1}) - \hat{x}_i^*(k_i^{m+1}|k_i^m)\|_{P_i} \\ &\quad + \sum_{s=0}^{l-1} L_{f_i}^s NL_{g_{ij}}\|\tilde{x}_j(k_i^{m+1}+s|k_i^{m+1}) - \tilde{x}_j(k_i^{m+1}+s|k_i^m))\|_{P_i} \end{aligned} \tag{17}$$

Let $\zeta_j(k) = \|\tilde{x}_j(k|k_i^{m+1}) - \tilde{x}_j(k|k_i^m))\|_{P_i}$. Based on (17), the triggering condition for feasibility is designed as follows.

$$\bar{k}_i^{m+1} = \inf_k \left\{k : L_{f_i}^{T_p-(k-k_i^m)+1}\|x_i(k) - \hat{x}_i^*(k|k_i^m)\|_{P_i} > L_{f_i}^{T_p-(k-k_i^m)+1}\delta_i - \sum_{s=0}^{T-(k-k_i^m)} L_{f_i}^s NL_{g_{ij}}\zeta_j(k+s)\right\} \tag{18a}$$

$$k_i^{m+1} = \min\{\bar{k}_i^{m+1}, k_i^m + T_p\}, \tag{18b}$$

where the right of (18a) is the triggering threshold, $\delta_i = (\eta_i - NL_{g_{ij}}(\eta_j + T_p\rho_j) - \xi_i)/L_{f_i}$ is the control parameter of subsystem i, and $\eta_i > 0$ is a to be designed control parameter.

Considering the asynchronous triggering mechanism and recalling (8), the control input applied to subsystem i is

$$u_i(k) = v_i^*(k|k_i^m) - H_i(x_i^*(k|k_i^m))\sum_{j\in\mathcal{N}_i} g_{ij}(\tilde{x}_j(k|k_i^m)). \tag{19}$$

The CSCT-based ET-DMPC strategy is summarized in Algorithm 1.

Algorithm 1: CSCT-Based Event-Triggered Distributed MPC.

1: Initialization: Let $m=0$, the initial state $x_i(k_i^0)$, and the related parameters $T, Q_i, R_i, P_i, \varepsilon_i$.
2: **if** the triggering condition in (18) are satisfied **then**
3: Set the triggering instant $m=m+1, k_i^m=k$;
4: Subsystems i solves the optimization problem in (12) to generate $\hat{\mathbf{v}}_i^*(k_i^m)$ and $\hat{\mathbf{x}}_i^*(k_i^m)$, and transmits $\hat{\mathbf{x}}_i^*(k_i^m)$ to its neighbors;
5: **end if**
6: Apply the control input in (19) to subsystem i;
7: Set $k=k+1$, and go to 2.

Remark 5: The proposed triggering condition offers two primary advantages over traditional trigger conditions: (a) the state prediction error, denoted as $\|x_i(k)-\hat{x}_i^*(k|k_i^m)\|_{P_i}$, is reduced by CSCT; (b) a larger triggering threshold can be attained due to the following reasons: (i) The value of $L_{f_i}^{T_p-(k-k_i^m)+1}\delta_i$ escalates as k progresses. (ii) The parameter associated with the neighboring system, $L_{g_{ij}}$, is constrained such that $L_{g_{ij}} \le \bar{L}_{g_{ij}}$, facilitated by the CSCT, thereby mitigating the conservativeness inherent in the parameter design.

IV. Analysis

In this section, the recursive feasibility of the optimization problem (12) is analyzed, followed by the analysis of the satisfaction of actual state constraint and the stability for the system.

A. Recursive Feasibility Analysis

Recursive feasibility means that the solution to the optimization problem (12) always exists at each triggering instant. Before presenting the result to guarantee the recursive feasibility, an assumption is given to facilitate the initial feasibility.

Assumption 4: There exist assumed sate trajectory $\tilde{\mathbf{x}}_j(0), j\in\mathcal{N}_i$ such that the optimization problem (12) has a feasible solution.

Theorem 1: For the subsystem (1) with Assumptions 1–4 and the triggering condition (18) is adopt, if the following conditions

$$\frac{1-L_{f_i}^{T_p}}{1-L_{f_i}} N L_{g_{ij}}\rho_j + L_{f_i}^{T_p}\eta_i \le \rho_i \tag{20}$$

$$\rho_i \le (1-\alpha_i)\varepsilon_i \tag{21}$$

are satisfied, the optimization problem (12) is recursively feasible.

Proof: We prove recursive feasibility using the principle of mathematical induction. Specifically, assuming that the optimization problem has a solution at k_i^m, denoted by $\hat{\mathbf{v}}_i^*(k_i^m)$, we need to demonstrate that the constructed control input sequence $\bar{\boldsymbol{v}}_i(k_i^{m+1}+l|k_i^{m+1})$ defined in (16) is a feasible solution at k_i^{m+1}.

First, we derive the upper bound of the predicted error at the next triggering instant, which facilitates the recursive feasibility analysis. Based on the triggering condition given in (18), we have

$$\|x_i(k_i^{m+1}-1)-\hat{x}_i^*(k_i^{m+1}-1|k_i^m)\|_{P_i}\le\delta_i.$$

Therefore, we can derive that:

$$\begin{aligned}
&\|x_i(k_i^{m+1})-\hat{x}_i^*(k_i^{m+1}|k_i^m)\|_{P_i}\\
&\le L_{f_i}\|x_i(k_i^{m+1}-1)-\hat{x}_i^*(k_i^{m+1}-1|k_i^m)\|_{P_i}+\xi_i\\
&\quad+NL_{g_{ij}}\|x_j(k_i^{m+1}-1)-\tilde{x}_j(k_i^{m+1}-1|k_i^m)\|_{P_i}\\
&\le L_{f_i}\delta_i+\xi_i\\
&\quad+NL_{g_{ij}}\|x_j(k_i^{m+1}-1)-\hat{x}_j^*(k_i^{m+1}-1|\pi(k_i^{m+1}-1))\\
&\quad+\hat{x}_j^*(k_i^{m+1}-1|\pi(k_i^{m+1}-1))-\tilde{x}_j(k_i^{m+1}-1|k_i^m)\|_{P_i}
\end{aligned}$$

Since $\delta_i=(\eta_i-NL_{g_{ij}}(\eta_j+T_p\rho_j)-\xi_i)/L_{f_i}$, we have

$$\|x_i(k_i^{m+1})-\hat{x}_i^*(k_i^{m+1}|k_i^m)\|_{P_i}\le\eta_i \tag{22}$$

In the sequel, the feasibility is verified from the following four aspects:

- $\bar{x}_i\,(k_i{}^{m+1}+l|k_i^{m+1})\in\Xi_i(l)$, $\forall l=1,\ldots,T_p-1$. This proof can be divided into two parts. For $l=1,\ldots,T_p-\Delta(k_i{}^m)$, according to (17) and (22), we have $\|\bar{x}_i\,(k_i^{m+1}+l|k_i{}^{m+1})\|_{P_i}\le\|\hat{x}_i{}^*(k_i{}^{m+1}+l|k_i{}^m)\|_{P_i}+L_{f_i}{}^l\eta_i+\sum_{s=0}{}^{l-1}L_{f_i}{}^sNL_{g_{ij}}\rho_j$. Due to $\hat{x}_i{}^*(k_i^{m+1}+l|k_i^m)\in\Xi_i(l+\Delta(k_i{}^m))$, it holds that $\bar{x}_i(k_i{}^{m+1}+l|k_i{}^{m+1})\in\Xi_i(l+\Delta(k_i{}^m))\oplus+L_{f_i}{}^l\eta_i+\sum_{s=0}{}^{l-1}L_{f_i}{}^sNL_{g_{ij}}\rho_j\subset\Xi_i(l)$.
  For $l=T_p-\Delta(k_i^m)+1,\ldots,T_p-1$, substituting $l=T_p-\Delta(k_i^m)$ into (17) and using triangle inequality, we can obtain that $\|\bar{x}_i\,(k_i{}^m+T|k_i{}^{m+1})\|_{P_i}\le\|\hat{x}_i{}^*(k_i^m+T|k_i^m)\|_{P_i}+L_{f_i}{}^{T_p-\Delta(k_i^m)}\eta_i+\sum_{s=0}^{T-\Delta(k_i^m)-1}L_{f_i}^sNL_{g_{ij}}\rho_j$.
  Since $\hat{x}_i{}^*(k_i{}^m+T_p|k_i{}^m)\in\phi_i(\alpha_i\varepsilon_i)$, using (20) and (21), it follows that $\bar{x}_i\,(k_i^m+T_p|k_i^{m+1})\in\phi_i(\varepsilon_i)$. Then, using Assumption 3, we have $\bar{x}_i(k_i{}^{m+1}+l|k_i{}^{m+1})\in\phi_i(\varepsilon_i)\subseteq\Xi_i(l)$, $\forall l=T_p-\Delta(k_i^m)+1,\ldots,T_p-1$.
- $\|\bar{x}_i(k_i^{m+1}+l|k_i^{m+1})-\hat{x}_i^*(k_i^{m+1}+l|k_i^m)\|_{P_i}\le\rho_i$. Combining (17), (20) and (22), this can be derived.
- $\bar{x}_i(k_i^{m+1}+T_p|k_i^{m+1})\in\phi_i(\alpha_i\varepsilon_i)$. From the above proof, we have $\bar{x}_i(k_i^m+T_p|k_i^{m+1})\in\phi_i(\varepsilon_i)$. Therefore, by virtue of Assumption 3, it ensures that $\bar{x}_i(k_i^{m+1}+T_p|k_i^{m+1})$ belongs to the terminal set $\phi_i(\alpha_i\varepsilon_i)$.
- $\bar{v}_i(k_i^{m+1}+l|k_i^{m+1})\in\mathcal{U}_i-\mathcal{V}_i$. This can be directly verified by $\hat{v}_i^*(k_i^m+l+\Delta(k_i^m)|k_i^m)\in\mathcal{U}_i-\mathcal{V}_i$, and $K_ix_i\in\mathcal{U}_i-\mathcal{V}_i$.

This proof is completed. ■

From the above analysis, the proposed CSCT achieves significant improvements in prediction accuracy. Furthermore, as established in Theorem 1, the algorithm maintains recursive feasibility while enabling enhanced inter-subsystem coupling tolerance through the reduction of coupling gain coefficients $L_{g_{ij}}$. This critical property relaxes conventional coupling strength constraints, thereby expanding the algorithm's applicability to CPSs with intensified dynamic interactions.

Remark 6: Theorem 1 gives the basis for the selection of the prediction horizon T_p, the control parameters ρ_i and η_i.

1) From (20), it can be derived that a larger prediction horizon T_p leads to a smaller η_i, resulting in a smaller triggering threshold δ_i ($\delta_i = (\eta_i - NL_{g_{ij}}(\eta_j + T\rho_j) - \xi_i)/L_{f_i}$), although a larger T_p has the potential to improve the control performance.
2) To select the control parameters, one can first determine ρ_i according to (21), and then choose appropriate T_p, η_i, and ρ_j based on (20).

B. Actual State Constraint

Theorem 2: Suppose that Assumption 1–3 hold. Under Algorithm 1, the actual state constraint $x_i(k) \in \mathcal{X}_i$ is satisfied.

Proof: The actual state trajectory is generated by employing the control input $u(k), k \in [k_i^m, k_i^{m+1} - 1]$ defined in (19). Therefore, we only need to prove that $x_i(k) \in \mathcal{X}_i, \forall k \in [k_i^m, k_i^{m+1} - 1]$. According to (18) and (22), we have $\|x_i(k_i^m + l)\|_{P_i} \le \|\hat{x}_i^*(k_i^m + l|k_i^m)\|_{P_i} + \eta_i$. Since $\hat{x}_i^*(k_i^m + l|k_i^m) \in \Xi_i(l)$, we can obtain that $x_i(k_i^m + l) \in \Xi_i(l) \oplus \eta_i \subseteq \mathcal{X}_i$, which completes this proof. ■

C. Stability Analysis

Theorem 3: Suppose that Assumptions 1–4 hold and the conditions in Theorem 1 are satisfied, then the closed-loop system is ISpS under Algorithm 1.

Proof: According to the definition in [26], one needs to show that there exist $\mathcal{KL}$-function β, $\mathcal{K}$-function γ, and a nonnegative constant d such that $\|x_i(k)\| \le \beta(\|x_i(k_i^0)), k - k_i^0\|) + \gamma(\|w\|) + d$ holds. To that end, we can choose candidate ISpS-Lyapunov function $V_i(x_i(k))$ and then prove that there exist functions $\eta_1, \eta_2, \eta_3 \in \mathcal{K}_\infty$, $\varrho \in \mathcal{K}$, and a constant $d \ge 0$ such that: (i) $\eta_1(\|x_i(k)\|) \le V_i(x_i(k)) \le \eta_2(\|x_i(k)\|)$, and (ii) $V_i(x_i(k+1) - V_i(x_i(k)) \le -\eta_3(\|x_i(k)\|) + \varrho(\|w\|) + d$ holds. We choose $V_i(x_i(k)) = J_i(x_i(k + l|k), v_i(k + l|k))$ at time k. In particular, if $k = k_i^m$, then $V_i(x_i(k)) = J_i(\hat{x}_i^*(k_i^m + l|k_i^m), \hat{v}_i^*(k_i^m + l|k_i^m))$. The control input $v_i(k + m|k)$ is constructed in the same manner as in (16). According to [27], $\eta_1(\|x_i(k)\|) \le V_i(x_i(k)) \le \eta_2(\|x_i(k)\|)$ can be easily obtained. The rest mainly proves (ii). For $k = k_i^m$, we can derive that

$$\begin{aligned}
&V_i(x_i(k+1)) - V_i(x_i(k)) \\
\le\ & -\psi(\hat{x}_i^*(k_i^m|k_i^m), \hat{v}_i^*(k_i^m|k_i^m)) \\
&+ \sum_{l=1}^{T_p-1} (\psi(\bar{x}_i(k+l|k+1), \bar{v}_i(k+l|k+1)) \\
&- \psi(\hat{x}_i^*(k+l|k_i^m), \hat{v}_i^*(k+l|k_i^m))) \\
&+ \psi(\bar{x}_i(k+T_p|k+1), \bar{v}_i(k+T_p|k+1) \\
&+ \varphi(\bar{x}_i(k+1+T_p|k+1)) - \varphi(\hat{x}_i^*(k_i^m + T_p|k_i^m)) \quad (23)
\end{aligned}$$

Let $\Delta_1 = \sum_{l=1}^{T_p-1} (\psi(\bar{x}_i (k+l|k+1), \bar{v}_i (k+l|k+1)) - \psi(\hat{x}_i^* (k+l|k_i^m), \hat{v}_i^* (k+l|k_i^m)))$ and $\Delta_2 = \psi(\bar{x}_i (k+T_p|k+1), \bar{v}_i(k+T_p|k+1) + \varphi(\bar{x}_i (k+1+T_p|k+1)) - \varphi(\hat{x}_i^* (k_i^m + T_p|k_i^m))$. Since $\bar{v}_i (k+l|k+1) = \hat{v}_i^* (k+l|k_i^m)$, $\forall l = 1, \ldots, T_p - 1$, we have

$$\begin{aligned}
\Delta_1 &\le \sum_{l=1}^{T_p-1} L_\psi \|\bar{x}_i(k+l|k+1) - \hat{x}_i^*(k+l|k_i^m)\|_{P_i} \\
&\le \sum_{l=1}^{T_p-1} L_\psi (L_{f_i}^{l-1} \|x_i(k+1) - \hat{x}_i^*(k+1|k_i^m)\|_{P_i} \\
&\quad + \sum_{s=0}^{l-2} L_{f_i}^s N L_{g_{ij}} |\tilde{x}_j(k_i^{m+1} + s|k_i^{m+1}) \\
&\quad - \tilde{x}_j(k_i^{m+1} + s|k_i^m))\|_{P_i})
\end{aligned}$$

Let $w_i(k) = \|x_i(k) - \hat{x}_i^*(k|k_i^m)\|_{P_i}$, we further obtain

$$\Delta_1 \le \sum_{l=1}^{T_p-1} L_\psi \left(L_{f_i}^{l-1} \|w_i(k+1)\|_{P_i} + \sum_{s=0}^{l-2} L_{f_i}^s N L_{g_{ij}} \rho_j \right)$$

Since $\bar{x}_i(k + T_p|k + 1) \in \phi_i(\varepsilon_i)$, by virtue of Assumption 3, we can derive that

$$\begin{aligned}
\Delta_2 &= \psi(\bar{x}_i(k+T_p|k+1), \bar{v}_i(k+T_p|k+1) - \varphi(\hat{x}_i^*(k_i^m + T_p|k_i^m)) \\
&\quad + \varphi(\bar{x}_i(k+1+T_p|k+1)) \\
&\le \varphi(\bar{x}_i(k+T_p|k+1)) - \varphi(\hat{x}_i^*(k_i^m + T_p|k_i^m)) \\
&\quad + \varphi\left(\sum_{j \in \mathcal{N}_i} g_{ij}^U(\tilde{x}_j(k+T_p|k+1)) \right) \\
&\le L_\varphi \left(L_{f_i}^{T_p-1} \|w_i(k+1)\|_{P_i} + \sum_{s=0}^{T_p-2} L_{f_i}^s N L_{g_{ij}} \rho_j \right) + L_\varphi N L_{g_{ij}} \varepsilon_j
\end{aligned}$$

where L_φ is a constant such that $\varphi(x) - \varphi(y) \le L_\varphi(x - y), \forall x, y \in \mathcal{X}_i$ holds.

Summarize the above analysis, we can further obtain that $V_i(x_i(k+1)) - V_i(x_i(k)) \le \eta_3(\|x_i(k)\|) + \varrho(\|w\|) + d$, where $\eta_3(s) = \|s\|_{Q_i}^2$, $\varrho(s) = \left(\frac{L_\psi(1 - L_{f_i}^{T_p-1})}{1 - L_f} + L_\varphi L_{f_i}^{T_p-1} \right) \|s\|_{P_i}^2$, and $d = \left(\sum_{l=1}^{T_p-1} L_\psi \frac{(1 - L_{f_i}^{l-1})}{1 - L_f} + L_\varphi \frac{(1 - L_{f_i}^{T_p-1})}{1 - L_f} \right) N L_{g_{ij}} \rho_j + L_\varphi N L_{g_{ij}} \varepsilon_j$. ■

V. Simulation Example

A. Example 1

In this section, the effectiveness of the proposed CSCT-based ET-DMPC strategy is validated through the nonlinear version of the CPS in [28]. The dynamics of the three carts are

$$\begin{aligned}
x_{11}(k+1) &= x_{11}(k) + \tau x_{12}(k) \\
x_{12}(k+1) &= (1 - \frac{\tau h_d}{m_c}) x_{12}(k) - \frac{\tau k_s}{m_c} e^{-x_{11}(k)} x_{11}(k) \\
&\quad - \frac{\tau k_c}{m_c}(x_{11}(k) - x_{21}(k)) + \frac{\tau}{m_c} u_1 + \omega_1(k) \\
x_{21}(k+1) &= x_{21}(k) + \tau x_{22}(k)
\end{aligned}$$

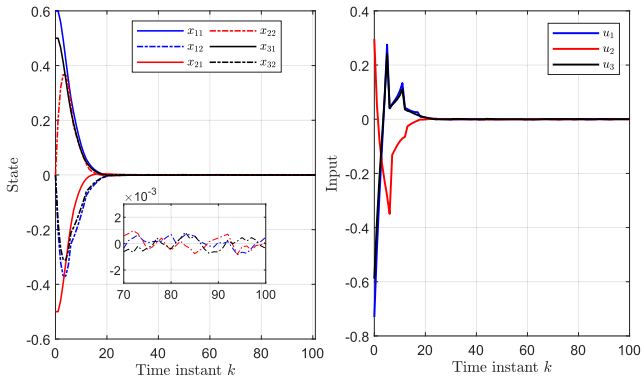

Fig. 2. State and control input trajectories under Algorithm 1.

$$x_{22}(k+1) = (1 - \frac{\tau h_d}{m_c})x_{22}(k) - \frac{Tk_s}{m_c}e^{-x_{21}(k)}x_{21}(k) - \frac{\tau k_c}{m_c}(x_{21}(k) - x_{11}(k)) - \frac{\tau k_c}{m_c}(x_{21}(k) - x_{31}(k)) + \frac{\tau}{m_c}u_2 + \omega_2(k)$$

$$x_{31}(k+1) = x_{31}(k) + \tau x_{32}(k)$$

$$x_{32}(k+1) = (1 - \frac{\tau h_d}{m_c})x_{32}(k) - \frac{\tau k_s}{m_c}e^{-x_{31}(k)}x_{31}(k) - \frac{\tau k_c}{m_c}(x_{31}(k) - x_{21}(k)) + \frac{\tau}{m_c}u_3 + \omega_3(k)$$

where x_{i1} and x_{i2} represent the displacement and velocity of cart $i, i = 1, 2, 3$, respectively; k_s and h_d denote the stiffness of the local nonlinear spring and the local viscous damping of each cart i, respectively; k_c represents the stiffness of the interconnecting springs; m_c is the mass of each cart; u_i is the control signal; and ω_i is the disturbance. τ is the sampling time. $k_s = 0.8$ N/m, $h_d = 1$ Ns/m, $k_c = 0.03$ N/m, and $m_c = 1$ kg. The state and control input constraints for each cart are $\mathcal{X}_i = \{x_i : -1 \le x_{i1} \le 1, -1 \le x_{i2} \le 1\}$ and $\mathcal{U}_i = \{u_i : -1 \le u_i \le 1\}$, respectively. The disturbance bounds are $\xi_1 = \xi_2 = \xi_3 = 0.0005$. The initial states are $x_1(0) = (0.6, 0)$, $x_2(0) = (-0.5, 0)$, and $x_3(0) = (0.5, 0)$.

To implement the algorithm, the weighted matrices are chosen as $Q_i = [0.2\ 0; 0\ 0.2]$, and $R_i = 0.1$, $i = 1, 2, 3$. To satisfy Assumption 3, the feedback control law is calculated as $K_1 = K_3 = [-0.6062 - 1.0914]$, $K_2 = [-0.5902 - 1.0872]$. The terminal weighted matrices are calculated as $P_1 = P_2 = [3.4123\ \ 0.9963; 0.9963\ \ 1.6437]$, and $P_3 = [3.4149\ \ 0.9878; 0.9878\ \ 1.6423]$. The other parameters are $L_{f_i} = 1.19$, $\varepsilon_i = 0.6$, $\alpha_i = 0.97$, $i = 1, 2, 3$. Note that there are no unmatched couplings in this system, therefore $\sum_{j \in \mathcal{N}_i} g_{ij}^U(x_j(k)) = 0$. According to Theorem 1, the other control parameters can be chosen as $T_p = 6$, $\rho_i = 0.00852$, $\eta_i = 0.003$, $i = 1, 2, 3$. Therefore $\delta_i = 0.0021$.

As demonstrated in Fig. 2, the state and control input trajectories are generated under Algorithm 1. Fig. 3 illustrates the evolution of the Lyapunov function, which exhibits a decreasing trend toward zero over time. Together, Figs. 2 and 3 serve as evidence

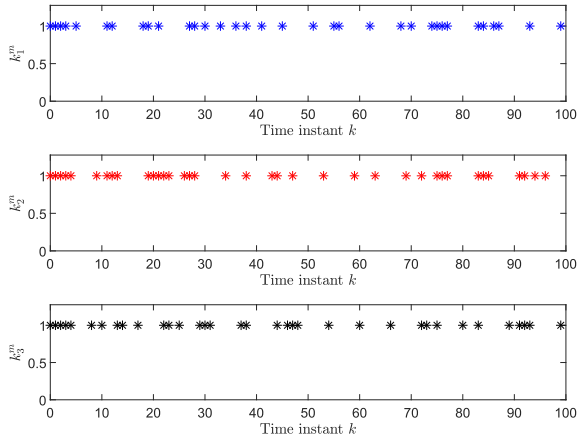

Fig. 3. Triggering instants under the ET-DMPC algorithm in [18].

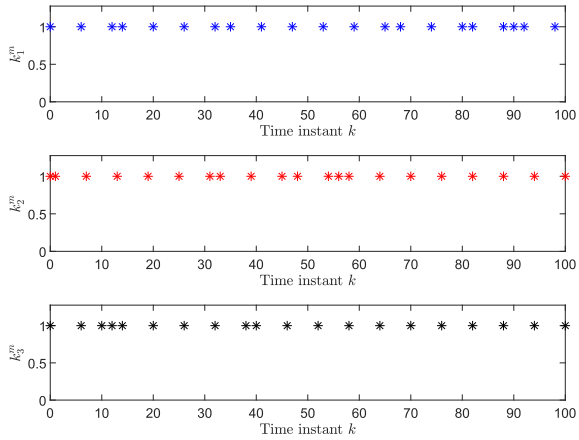

Fig. 4. Triggering instants under Algorithm 1.

that the overall system achieves ISpS under the Algorithm 1, and the state and control input constraints are satisfied. To validate the effectiveness of the proposed strategy in alleviating communication load and ensuring control performance, trigger frequency and control performance, as used in many event-triggered MPC studies [6], [16], are introduced. We compare the number of triggering instants and control performance under Algorithm 1 with those under the ET-DMPC algorithm in [18]. Note that $\sum_{j \in \mathcal{N}_i} g_{ij}^U(x_j(k)) \neq 0$ in [18] without CSCT. As a result, if $\rho_i = 0.00852$, then $\eta_i = 0.0026$ (and thus $\delta_i = 0.0012$) to guarantee recursive feasibility. Define the performance index

$$J(k) = \sum_{i \in \mathcal{N}} \sum_{l=0}^{T_{sim}} (\|x_i(k)\|_{Q_i}^2 + \|u_i(k)\|_{R_i}^2), \tag{24}$$

where T_{sim} is the simulation steps. Figs. 3 and 4 illustrate the number of triggers for Algorithm 1 and the ET- DMPC algorithm in [18]. Over 300 steps, Algorithm 1 has 60 triggering instances compared to 108 in [18]. This represents a 44% reduction in triggers for Algorithm 1, highlighting its communication - burden - alleviating advantage. Additionally, the values of J corresponding to Figs. 3 and 4 are 1.4073 and 1.4235, respectively. We can find that the proposed strategy reduces the triggering frequency more efficiently and achieves comparable control performance.

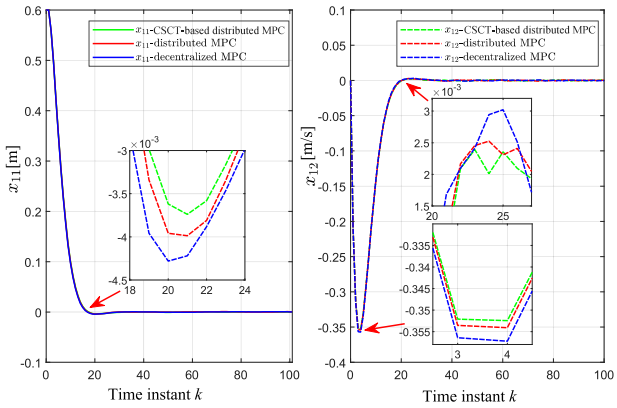

Fig. 5. The comparison of x_1.

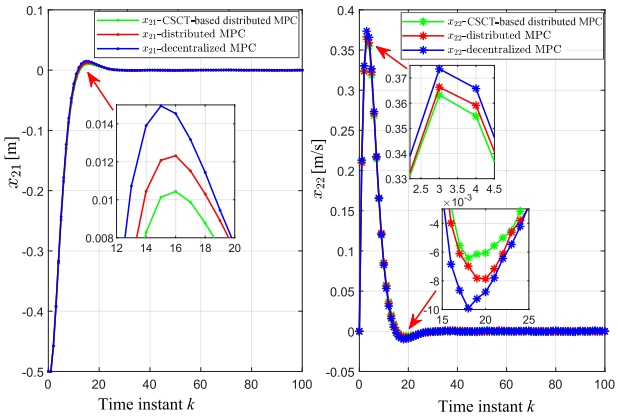

Fig. 6. The comparison of x_2.

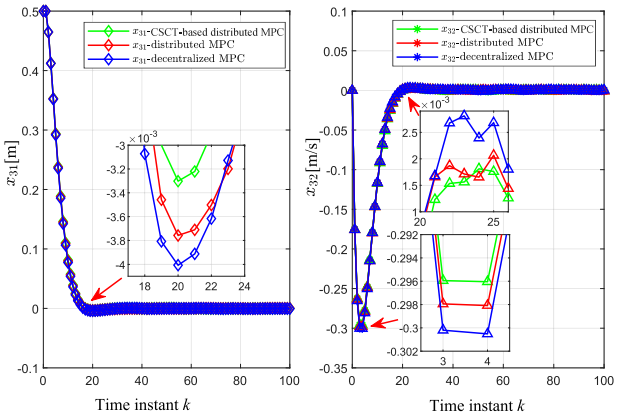

Fig. 7. The comparison of x_3.

Furthermore, to demonstrate the advantage of the proposed CSCT-based distributed MPC in enhancing prediction precision, we compare the state trajectories generated by the CSCT-based distributed MPC algorithm, the distributed MPC algorithm, and the decentralized MPC algorithm, as shown in Figs. 5 –7. It can be observed that the proposed CSCT-based distributed MPC algorithm achieves higher prediction precision.

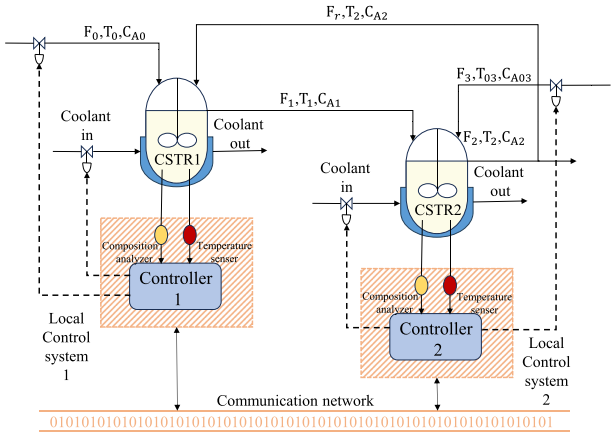

Fig. 8. Process flow diagram of two interconnected CSTRs.

B. Example 2

An example of interconnected CPS, chemical reactors with recycle, borrowed from [23], [29], is provided to show the effectiveness of the proposed CSCT-based ET-DMPC strategy. The plant consists of two non-isothermal continuous stirred-tank reactors (CSTRs) with uniform mixing, and the reactors are connected to each other. Fig. 8 shows the process flow diagram of the CSTRs. The plant model is given as

$$\dot{T}_1 = \frac{F_0}{V_1}(T_0 - T_1) + \frac{F_r}{V_1}(T_2 - T_1) + \sum_{i=1}^{3} G_i(T_1)C_{A1} + \frac{O_1}{\rho c_p V_1},$$

$$\dot{C}_{A1} = \frac{F_0}{V_1}(C_{A0} - C_{A1}) + \frac{F_r}{V_1}(C_{A2} - C_{A1}) - \sum_{i=1}^{3} R_i(T_1)C_{A1},$$

$$\dot{T}_2 = \frac{F_1}{V_2}(T_1 - T_2) + \frac{F_3}{V_2}(T_{03} - T_2) + \sum_{i=1}^{3} G_i(T_2)C_{A2} + \frac{O_2}{\rho c_p V_2},$$

$$\dot{C}_{A2} = \frac{F_1}{V_2}(C_{A1} - C_{A2}) + \frac{F_3}{V_2}(C_{A03} - C_{A2}) - \sum_{i=1}^{3} R_i(T_2)C_{A2}.$$

where T_i denotes the fluid temperature in CSTR i, C_{Ai} denotes fluid molar concentration of CSTR i, O_i is heat input rates of the corresponding CSTR i, and V_i denotes volume of CSTR i for $i = 1, 2$. $G_i(T_j) = \frac{-\Delta H_i}{\rho c_p} R_i(T_j)$, $R_i(T_j) = k_{i0} \exp(-\frac{E_i}{RT_j})$, $j = 1, 2$. Temperature T_0 and molar concentration C_{A0}, C_{A03} are re known constant parameters. ρ and c_p denote the density and heat capacity of fluid in the reactor, respectively. The system parameters are chosen as [23]. The open loop plant is unstable at the desired operating in which $(T_1, C_{A1}, T_2, C_{A2}) =$ (324 K, 0.718 $\mathrm{kmol/m^3}$,324 K,0.432 $\mathrm{kmol/m^3}$). The state and control constraints for each CSTR are 250 K $\leq T_i \leq$ 400 K, $0 \leq CA_i \leq 1\,\mathrm{kmol/m^3}$, and $\|Q_i\| \leq 10^6$.

With the sampling time 0.003 h, the system is discretized to obtain the discre-time dynamic (1), where $x_1 = [T_1,\ C_{A1}]^T$, $x_2 = [T_2,\ C_{A2}]^T$, $u_1 = O_1$, and $u_2 = O_2$. To implement the algorithm, the weighted matrices are chosen as $Q_i = [10^{-10}\ \ 0; 0\ \ 10^{-2}]$, and $R_i = 10^{-15}$,

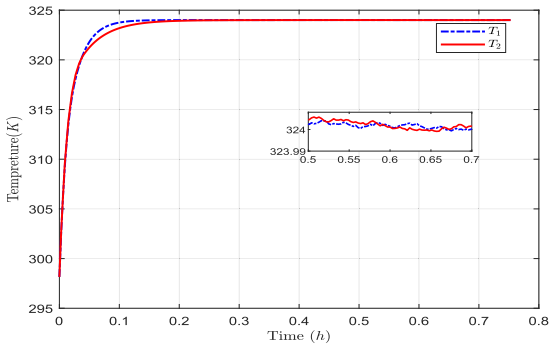

Fig. 9. Temperature of each CSTR.

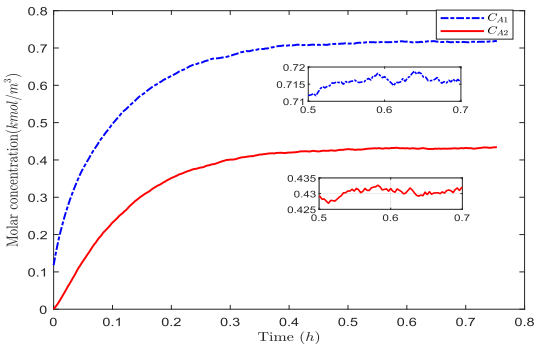

Fig. 10. Molar concentration of each CSTR.

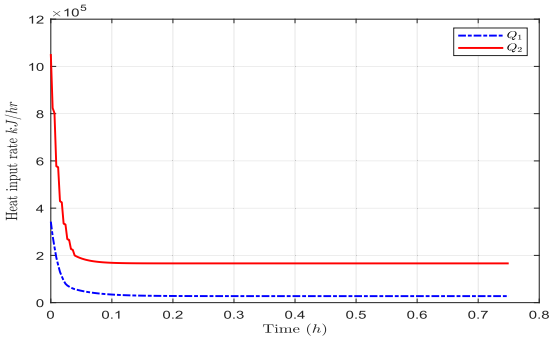

Fig. 11. Heat input rate of each CSTR.

$i = 1, 2$. To satisfy Assumption 3, the feedback control law is calculated as $K_1 = [-5.0325 \ \ 631.7778]$, $K_2 = [-2.8919 \ \ 385.4584]$. The terminal weighted matrices are calculated as $P_1 = [0.0886 \ \ 0.0034; 0.0034 \ \ 0.9317]$, and $P_2 = [0.1480 \ \ 0.0034; 0.0034 \ \ 1.5556]$. The other parameters are $L_{f_i} = 1.05$, $\varepsilon_i = 0.9$, $\alpha_i = 0.95$, $i = 1, 2$. Note that there are no unmatched couplings in this system, therefore $\sum_{j\in\mathcal{N}_i} g_{ij}^U(x_j(k)) = 0$. According to Theorem 1, the other control parameters can be chosen as $T_p = 6$, $\rho_i = 0.0474$, $\eta_i = 0.0354$, $i = 1, 2$. Therefore $\delta_i = 0.0328$.

The simulation results are shown in Figs. 9–13. From Figs. 9–11, it can be seen that constraints temperature and molar concentration are satisfied, and constraints temperature and molar concentration can quickly return to the desired operating point.

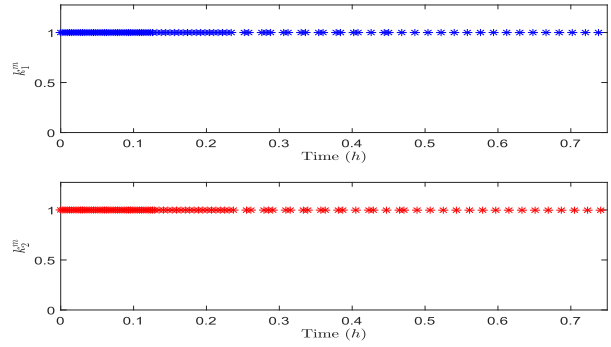

Fig. 12. Triggering instants under the ET-DMPC algorithm in [18].

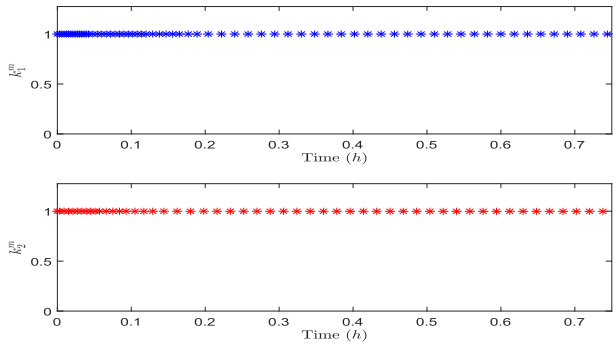

Fig. 13. Triggering instants under Algorithm 1.

We also compared the number of triggering instants and control performance index in (24) under the proposed Algorithm 1 with those under the ET-DMPC algorithm in [18], see Figs. 12 and 13. Note that $\sum_{j\in\mathcal{N}_i} g_{ij}^U(x_j(k)) \neq 0$ in [18] without CSCT. As a result, $\delta_i = 0.0048$ to guarantee recursive feasibility. The value of J corresponding to Figs. 12 and 13 are 0.1003 and 0.1019, respectively. Therefore, in terms of reducing the trigger frequency, proposed Algorithm 1 can reduce the trigger by 38% compared to the latest algorithm in [18], while obtain comparable control performance.

VI. Conclusion

In this paper, a novel ET-DMPC strategy based on CSCT has been investigated for CPSs with coupled dynamics. With this strategy, the prediction precision has been enhanced and the triggering threshold has been enlarged, thereby the triggering frequency has been reduced significantly, saving communication resources. Sufficient conditions to ensure the recursive feasibility and ISpS have been established.

References

[1] S. Guarino, F. Vitale, F. Flammini, L. Faramondi, N. Mazzocca, and R. Setola, "A two-level fusion framework for cyber-physical anomaly detection," *IEEE Trans. Ind. Cyber- Phys. Syst.*, vol. 2, pp. 1–13, 2023.

[2] D. Zhao, Y. Shi, S. X. Ding, Y. Li, and F. Fu, "Replay attack detection based on parity space method for cyber-physical systems," *IEEE Trans. Autom. Control*, vol. 70, no. 4, pp. 2390–2405, Apr. 2025.

[3] Y. Dai, M. Li, K. Zhang, and Y. Shi, "Robust and resilient distributed MPC for cyber-physical systems against DoS attacks," *IEEE Trans. Ind. Cyber-Phys. Syst.*, vol. 1, pp. 44–55, 2023.

[4] X. Liu, Y. Shi, and D. Constantinescu, "Distributed model predictive control of constrained weakly coupled nonlinear systems," *Syst. Control Lett.*, vol. 74, pp. 41–49, 2014.
[5] S. Huang, D. Sun, and M. Zhao, "Distributed MPC-based hierarchical cooperative control for mixed vehicle groups with T-CPS in the vicinity of traffic signal light," *IEEE Trans. Intell. Transp. Syst.*, vol. 25, no. 7, pp. 8003–8016, Jul. 2024.
[6] T. Wang, Y. Kang, P. Li, Y.-B. Zhao, and H. Tang, "Rolling self-triggered distributed MPC for dynamically coupled nonlinear systems," *Automatica*, vol. 160, 2024, Art. no. 111444.
[7] S. Riverso, M. Farina, and G. Ferrari-Trecate, "Plug-and-play decentralized model predictive control for linear systems," *IEEE Trans. Autom. Control*, vol. 58, no. 10, pp. 2608–2614, Oct. 2013.
[8] A. Mirzaei and A. Ramezani, "Cooperative optimization-based distributed model predictive control for constrained nonlinear large-scale systems with stability and feasibility guarantees," *ISA Trans.*, vol. 116, pp. 81–96, 2021.
[9] W. B. Dunbar, "Distributed receding horizon control of dynamically coupled nonlinear systems," *IEEE Trans. Autom. Control*, vol. 52, no. 7, pp. 1249–1263, Jul. 2007.
[10] A. Ma, K. Liu, Q. Zhang, and Y. Xia, "Distributed MPC for linear discrete-time systems with disturbances and coupled states," *Syst. Control Lett.*, vol. 135, 2020, Art. no. 104578.
[11] L. Dai, T. Zhou, Z. Qiang, Z. Sun, and Y. Xia, "Distributed economic MPC for dynamically coupled linear systems: A Lyapunov-based approach," *IEEE Trans. Syst., Man, Cybern. Syst.*, vol. 53, no. 3, pp. 1408–1419, Mar. 2023.
[12] H. Hu, K. Gatsis, M. Morari, and G. J. Pappas, "Non-cooperative distributed MPC with iterative learning," *IFAC-PapersOnLine*, vol. 53, no. 2, pp. 5225–5232, 2020.
[13] M. Kohler, J. Berberich, M. A. Müller, and F. Allgower, "Data-driven distributed MPC of dynamically coupled linear systems," *IFAC-PapersOnLine*, vol. 55, no. 30, pp. 365–370, 2022.
[14] Q. Sun, J. Chen, and Y. Shi, "Event-triggered robust MPC of nonlinear cyber-physical systems against DoS attacks," *Sci. China Inf. Sci.*, vol. 65, no. 1, 2022, Art. no. 110202.
[15] H. Li, W. Yan, Y. Shi, and Y. Wang, "Periodic event-triggering in distributed receding horizon control of nonlinear systems," *Syst. Control Lett.*, vol. 86, pp. 16–23, 2015.
[16] X. Mi, Y. Zou, and S. Li, "Event-triggered MPC design for distributed systems toward global performance," *Int. J. Robust Nonlinear Control*, vol. 28, no. 4, pp. 1474–1495, 2018.
[17] A. Ma, K. Liu, Q. Zhang, T. Liu, and Y. Xia, "Event-triggered distributed MPC with variable prediction horizon," *IEEE Trans. Autom. Control*, vol. 66, no. 10, pp. 4873–4880, Oct. 2021.
[18] C. Liu, H. Li, Y. Shi, and D. Xu, "Distributed event-triggered model predictive control of coupled nonlinear systems," *SIAM J. Control Optim.*, vol. 58, no. 2, pp. 714–734, 2020.
[19] Y. Zhou, D. Li, Y. Xi, and F. Gao, "Event-triggered distributed robust model predictive control for a class of nonlinear interconnected systems," *Automatica*, vol. 136, 2022, Art. no. 110039.
[20] T. Zhou, L. Dai, Q. Li, and Y. Xia, "Distributed economic MPC for dynamically coupled systems with stochastic disturbances," *IEEE Trans. Circuits Syst. I: Reg. Papers*, vol. 70, no. 12, pp. 5442–5455, Dec. 2023.
[21] Y. Kang, T. Wang, P. Li, Z. Xu, and Y.-B. Zhao, "Compound event-triggered distributed MPC for coupled nonlinear systems," *IEEE Trans. Cybern.*, vol. 53, no. 9, pp. 5572–5584, Sep. 2023.
[22] Q. Zhong, J. Yang, K. Shi, S. Zhong, Z. Li, and M. A. Sotelo, "Event-triggered H_∞ load frequency control for multi-area nonlinear power systems based on non-fragile proportional integral control strategy," *IEEE Trans. Intell. Transp. Syst.*, vol. 23, no. 8, pp. 12191–12201, Aug. 2021.
[23] Y. Zhang, F. Li, S. Gao, D. Zhao, X.-G. Yan, and S. K. Spurgeon, "Output consensus for interconnected heterogeneous systems via a combined model predictive control and integral sliding mode control with application to CSTRs," *Control Eng. Pract.*, vol. 153, 2024, Art. no. 106100.
[24] L. Dai, Z. Qiang, Z. Sun, T. Zhou, and Y. Xia, "Distributed economic MPC for dynamically coupled linear systems with uncertainties," *IEEE Trans. Cybern.*, vol. 52, no. 6, pp. 5301–5310, Jun. 2022.
[25] F. Castaños and L. Fridman, "Analysis and design of integral sliding manifolds for systems with unmatched perturbations," *IEEE Trans. Autom. Control*, vol. 51, no. 5, pp. 853–858, May 2006.
[26] Z.-P. Jiang, I. Mareels, and Y. Wang, "A Lyapunov formulation of nonlinear small gain theorem for interconnected systems," *IFAC Proc. Volumes*, vol. 28, no. 14, pp. 625–630, 1995.
[27] M. Wang, J. Sun, and J. Chen, "Input-to-state stability of perturbed nonlinear systems with event-triggered receding horizon control scheme," *IEEE Trans. Ind. Electron.*, vol. 66, no. 8, pp. 6393–6403, Aug. 2019.
[28] J. M. Bradley and E. M. Atkins, "Toward continuous state–space regulation of coupled cyber–physical systems," *Proc. IEEE*, vol. 100, no. 1, pp. 60–74, Jan. 2012.
[29] Y. Sun and N. H. El-Farra, "Quasi-decentralized model-based networked control of process systems," *Comput. Chem. Eng.*, vol. 32, no. 9, pp. 2016–2029, 2008.